

Tsallis' deformation parameter q quantifies the classical-quantum transition

A.M. Kowalski^{a,b}, M. T. Martin^{a,c}, A. Plastino^{a,c,*} and
L. Zunino^{d,e,a}

^a*Instituto de Física (IFLP-CCT-Conicet), Fac. de Ciencias Exactas,
Universidad Nacional de La Plata, C.C. 727, 1900 La Plata, Argentina*

^b*Comision de Investigaciones Científicas (CIC)*

^c*Argentina's National Research Council (CONICET)*

^d*Centro de Investigaciones Ópticas.
C.C. 124 Correo Central. 1900 La Plata, Argentina.*

^e*Departamento de Ciencias Básicas, Facultad de Ingeniería,
Universidad Nacional de La Plata (UNLP). 1900 La Plata, Argentina.*

Abstract

We investigate the classical limit of a type of semiclassical evolution, the pertinent system representing the interaction between matter and a given field. On using as a quantifier of the ensuing dynamics Tsallis q -entropy, we encounter that it not only appropriately describes the quantum-classical transition, but that the associated deformation-parameter q itself characterizes the different regimes involved in the process, detecting the most salient fine details of the changeover.

PACS: 89.70.Cf, 03.65.Sq, 05.45.Mt

KEYWORDS: Tsallis entropy, Semiclassical theories, quantum chaos, statistical complexity.

VERSION: 6.0

* Corresponding author. Phone / Fax.: +54-11-4786 8114

Email addresses: kowalski@fisica.unlp.edu.ar (A.M. Kowalski),
mtmartin@fisica.unlp.edu.ar (M. T. Martin), plastino@fisica.unlp.edu.ar
(A. Plastino), lucianoz@ciop.unlp.edu.ar (L. Zunino).

1 Introduction

1.1 Info-quantifiers

Quantifiers based on information theory, like entropic forms and statistical complexities (see as examples [1,2,3,4]) have proved to be quite useful in the characterization of the dynamics associated to time series, in the wake of the pioneering work of Kolmogorov and Sinai, who converted Shannon's information theory into a powerful tool for the study of dynamical systems [5,6].

Information theory measures and probability spaces Ω are inextricably linked. In the evaluation of above mentioned quantifiers, the determination of the probability distribution P associated to the dynamical system or time series under study is the basic element. Many procedures have been proposed for the election of $P \in \Omega$. We can mention techniques based on amplitude statistics [7], symbolic dynamics [8], Fourier analysis [9], and wavelet transform [10] (among others). The applicability of these approaches depends on data-characteristics, i.e., stationarity, length of the series, parameter-variations, levels of noise contamination, etc. The distinct treatments "capture" the global aspects of the dynamics, but they are not equivalent in their ability to discern physical details. However, one should recognize that we are here referring to techniques defined in an ad-hoc fashion, not derived directly from the dynamical properties of the pertinent system itself.

1.2 Deformed q -statistics

It is a well-known fact that physical systems that are characterized by either long-range interactions, long-term memories, or multi-fractality are best described by a generalized statistical mechanics' formalism [11] that was proposed 20 years ago, being usually alluded to as deformed q -statistics. More precisely, Tsallis [12] advanced in 1987 the idea of using in a thermodynamics' scenario an entropic the Harvda-Chavrat form, known today as Tsallis' q -entropy, characterized by the entropic index $q \in \mathcal{R}$ ($q \neq 1$):

$$S_q = \frac{1}{(q-1)} \sum_{i=1}^{N_s} [p_i - (p_i)^q], \quad (1)$$

where p_i are the probabilities associated with the associated N_s different system-configurations. The entropic index (or deformation parameter) q describes the deviations of Tsallis entropy from the standard Boltzmann-Gibbs-Shannon-one. Moreover, in the limit $q \rightarrow 1$ Tsallis' entropy reduces to Shan-

non's ¹

$$S = - \sum_{i=1}^{N_s} p_i \ln(p_i). \quad (2)$$

It is well-known that the orthodox entropy works best in dealing with systems composed of either independent subsystems or interacting via short-range forces whose subsystems can access all the available phase space [11]. For systems exhibiting long-range correlations, memory, or fractal properties, Tsallis' entropy becomes the most appropriate mathematical form [13,14,15,16,17,18,19,20,21,22,23].

1.3 Quantum-classical frontier

The classical limit of quantum mechanics (CLQM) continues attracting the attention of many theorists and is the source of much exciting discussion (see, for instance, Refs. [24,25] and references therein). In particular, the investigation of “quantum” chaotic motion is considered important in this limit. Recent literature provides us with many examples, although the adequate definition of the underlying phenomena is understood in diverse fashion according to the different authors (see Ref. [26] and references therein).

Our motivation derives from the fact that it should be reasonable to rely on q-statistics so as to gather insights into the

$$\text{quantum} - \text{semiclassical} - \text{classical transition}. \quad (3)$$

Why? Because we know that the classic to quantum route traverses high complexity regions of the appropriate phase space where chaos reigns, interrupted often by quasi-periodic windows [26,27,28]. In the semiclassical parcel of the associated trajectory one encounters also strong correlation between classical and quantum degrees of freedom [27,28]. The purpose of the present effort is precisely that of investigating the possible q-statistics' contribution to this problem. Since in this work the pertinent q-quantifiers are computed using “wavelet techniques”, we provide a brief wavelet-résumé in the Appendix.

2 A semi-classical model and the CLQM

Quite a bit of quantum insight is to be gained from semiclassical perspectives. Several methodologies are available (WKB, Born-Oppenheimer approach, etc.)

¹ When $q \rightarrow 1$, $p_i^{q-1} = e^{(q-1)\ln(p_i)} \sim 1 + (q-1)\ln(p_i)$.

Here we consider two interacting systems: a classical and a quantal ones. This can be done whenever the quantum effects of one of the two systems are negligible in comparison to those of the other one. Examples can be readily found. We can just mention Bloch-equations [29], two-level systems interacting with an electromagnetic field within a cavity, Jaynes-Cummings semiclassical model [30,31,32,33,34,35], collective nuclear motion [36], etc.

More recently [37,38,39], a special bipartite model has been employed with reference to problems in such diverse fields as chaos, wave-function collapse, measurement processes, and cosmology [40]. In order to tackle the problem posed at the very end of the Introduction we shall consider a trivial generalization of the semi-classical hamiltonian that represents the zero-th mode contribution of a strong external field to the production of charged meson pairs [38,39]. It reads

$$\hat{H} = \frac{1}{2} \left(\frac{\hat{p}^2}{m_q} + \frac{P_A^2}{m_{cl}} + m_q \omega^2 \hat{x}^2 \right), \quad (4)$$

where *i*) \hat{x} and \hat{p} are quantum operators, *ii*) A and P_A classical canonical conjugate variables and *iii*) $\omega^2 = \omega_q^2 + e^2 A^2$ is an interaction term that introduces nonlinearity, ω_q being a frequency. The quantities m_q and m_{cl} are masses, corresponding to the quantum and classical systems, respectively. As shown in Ref. [41], in dealing with (4) one faces an autonomous system of nonlinear coupled equations

$$\begin{aligned} \frac{d\langle \hat{x}^2 \rangle}{dt} &= \frac{\langle \hat{L} \rangle}{m_q}, & \frac{d\langle \hat{p}^2 \rangle}{dt} &= -m_q \omega^2 \langle \hat{L} \rangle, & \frac{d\langle \hat{L} \rangle}{dt} &= 2 \left(\frac{\langle \hat{p}^2 \rangle}{m_q} - m_q \omega^2 \langle \hat{x}^2 \rangle \right), \\ \frac{dA}{dt} &= \frac{P_A}{m_{cl}}, & \frac{dP_A}{dt} &= -e^2 m_q A \langle \hat{x}^2 \rangle, & \hat{L} &= \hat{x} \hat{p} + \hat{p} \hat{x}. \end{aligned} \quad (5)$$

The system of Eqs. (5) follows immediately from Ehrenfest's relations [41]. To study the classical limit we need to also consider the classical counterpart of the Hamiltonian (4)

$$H = \frac{1}{2} \left[\frac{p^2}{m_q} + \frac{P_A^2}{m_{cl}} + m_q (\omega_q^2 + e^2 A^2) x^2 \right], \quad (6)$$

where all the variables are classical. Recourse to Hamilton's equations allows one to find the classical version of Eqs. (5) (see Ref. [41] for details). The classical limit is obtained by letting the "relative energy"

$$E_r = \frac{|E|}{I^{1/2} \omega_q} \rightarrow \infty, \quad (7)$$

where E is the total energy of the system and I an invariant of the motion

described by the system (5), related to the Uncertainty Principle

$$I = \langle \hat{x}^2 \rangle \langle \hat{p}^2 \rangle - \frac{\langle \hat{L} \rangle^2}{4}. \quad (8)$$

A classical computation of I yields $I = x^2 p^2 - L^2/4 \equiv 0$. A measure of the convergence between classical and quantum results in the limit of Eq. (7) is given by the norm \mathcal{N} of the vector $\Delta u = u - u_{cl}$ [41]

$$\mathcal{N}_{\Delta u} = |u - u_{cl}|, \quad (9)$$

where the three components vector $u = (\langle \hat{x}^2 \rangle, \langle \hat{p}^2 \rangle, \langle \hat{L} \rangle)$ is the “quantum” part of the solution of the system Eqs. (5) and $u_{cl} = (x^2, p^2, L)$ its classical partner.

A detailed study of this model, was performed in Refs. [41,42]. We summarize here the main results of these references that are pertinent for our discussion. In plotting diverse dynamical quantities versus E_r (as it grows from unity to ∞), one finds *an abrupt change in the system’s dynamics for special values of E_r , to be denoted by E_r^{cl}* . From this value onwards, the pertinent dynamics starts converging to the classical one. It is thus possible to assert that E_r^{cl} provides us with an *indicator* of the presence of a quantum-classical “border”. The zone

$$E_r < E_r^{cl}, \quad (10)$$

corresponds to the semi-quantal regime investigated in Ref. [42]. This regime, in turn, is characterized by *two* different sub-zones [41]. *i)* One of them is an almost purely quantal one, in which the microscopic quantal oscillator is just slightly perturbed by the classical one, and *ii)* the other section exhibits a transitional nature (semi-quantal). The border between these two sub-zones can be well characterized by a “signal” value $E_r^{\mathcal{P}}$. A significant feature of this point resides in the fact that, for $E_r \geq E_r^{\mathcal{P}}$, *chaos is always found*. The relative number of chaotic orbits (with respect to the total number of orbits) grows with E_r and tends to unity for $E_r \rightarrow \infty$ [41,42].

Thus, as E_r grows from $E_r = 1$ (the “pure quantum instance”) to $E_r \rightarrow \infty$ (the classical situation), a significant series of *morphology-changes* is detected, specially in the transition-zone ($E_r^{\mathcal{P}} \leq E_r \leq E_r^{cl}$). The concomitant orbits exhibit features that are not easily describable in terms of Eq. (9), which is a *global* measure of convergence in amplitude (of the signal). What one needs instead is a statistical type of characterization, as that described in Refs. [27,28,43]. In the present work we will present a different, novel perspective of the quantum-classical transition problem and a characterization of it that we

believe to be more insightful and of a stronger convincing nature than those of [27,28,43].

3 Present results

By recourse to the so-called normalized Tsallis wavelet entropy (NTWE) \mathcal{H}_{S_q} given by (see Appendix)

$$\mathcal{H}_{S_q}[P] = S_q[P]/S_{q,max} = \frac{1}{1 - N_J^{1-q}} \sum_{j=-1}^{-N_J} (p_j - p_j^q), \quad (11)$$

we will be able to characterize the details that pave the road towards the classical limit.

In obtaining our numerical results we choose $m_q = m_{cl} = \omega_q = e = 1$ for the system's parameters. As for the initial conditions for solving the system (5) we take $E = 0.6$, i.e., we fix E and then vary I so to obtain our different E_r -values. Additionally, we have $\langle L \rangle(0) = L(0) = 0$ and $A(0) = 0$ (both in the quantum and the classical instances). $\langle x^2 \rangle(0)$ takes values in the interval $x^2(0) < \langle x^2 \rangle(0) \leq 0.502$, with $x^2(0) = 0.012$.

We define eight ($N_J = 8$) resolution levels $j = -1, -2, \dots, -N_J$ for an appropriate wavelet analysis within the multiresolution scheme. The p_j yield, at different scales, the energy probability distribution and so NTWE constitutes a suitable tool for detecting and characterizing specific phenomena.

We find as first result that the range of q values that allows for a correct description, is $0 < q < 5$ (see Figs. 1, 2 and 3, where we depicts the normalized Tsallis q entropy \mathcal{H}_{S_q} vs. E_r for different q-values). In this range \mathcal{H}_{S_q} distinguishes the three sections of our process, i.e., quantal, transitional, and classic, as delimited by, respectively, $E_r^{\mathcal{P}} = 3.3282$ and $E_r^{cl} = 21, 55264$. Notice the abrupt change of in the slope of the curve taking place at $E_r^{\mathcal{P}}$, where a local minimum is detected for $q > 0.1$ (Fig 1a). The transition zone is clearly demarcated between that point and E_r^{cl} . From here onwards \mathcal{H}_{S_q} adopts a "horizontal" behavior as it tends to its classical value at the same time that the solutions of (5) begin to converge towards the classical ones. If $q \geq 5$ two of our zones: transitional and classical, lose their identity (see below).

In general, the most noticeable \mathcal{H}_{S_q} - changes take place in the quantal zone, specially for $q < 1$ (Figs. 1a-b) and in the frontier between the transitional and classical zones, now for $q > 3$ (Fig. 3).

The \mathcal{H}_{S_q} –slope changes in the quantal sector as q varies, being negative for $q > 0.7$ (Figs. 1b, 2, and 3) and positive for $0 < q < 0.7$, if $E_r \leq 2.6$ (Figs. 1a). The slope is null in this last E_r –interval, for $q \simeq 0.7$ (Fig. 1b). Thus, for $q \leq \sim 0.4$, \mathcal{H}_{S_q} –values are, in the quantal zone, smaller (or equal) to those pertaining to the transitional one.

One concludes then that in the interval $0 < q \leq 0.4$, \mathcal{H}_{S_q} is able to represent in better fashion the quantal zone’s features than Shannon’s entropy (see [43]), as the information measure should be smaller in this zone than in the transitional one. In view of the meaning assigned to $E_r^{\mathcal{P}}$, it is then important to have a \mathcal{H}_{S_q} –minimum there. These considerations allow us to conclude that the optimal q –range is $0.1 < q \leq 0.4$.

For $0.7 \leq q < 1$, and as $q \rightarrow 1$, the q –entropy behavior resembles more and more the one of Shannon’s measure. No great changes ensue for $1 < q < 3$, while for $3 \leq q < 5$, the sharp demarcation of our three sections starts deteriorating. Notice in Fig. 3 that as q grows the \mathcal{H}_{S_q} –curve starts acquiring a “horizontal” nature in the transition region close to the classical one. A “merging” between the two sectors takes place for $q \geq 5$.

The q –influence on these processes is seen in Figs. 4, that plot \mathcal{H}_{S_q} vs. q for different values of our all important quantity E_r . The corresponding Shannon entropy value (horizontal line) is included in all graphs for comparison’s purpose. Typical kinds of morphology are exhibited by these figures [44]. Figs. 4a)–4b) correspond to the quantum sector, while Figs. 4c), 4d), 4e), and 4f) refer to the transitional one, and, finally, Figs. 4g)–4h) allude to the classical region. We verify that \mathcal{H}_{S_q} possesses only one minimum as a function of q . Consequently, \mathcal{H}_{S_q} intersects Shannon’s curve at two points, i.e., i) $q = 1$ and ii) another q –value, q^* , that depends on E_r . Note that $q^* < 1$ always, save for the $E_r = E_r^{\mathcal{P}}$ instance (in this case $q^* \simeq 2.55$). Figure 4c) depicts precisely this peculiar situation. The protagonist of Figs. 4d)–4e) is \mathcal{H}_{S_q} “tangency” to the Shannon entropy. Figure 4e) corresponds to $E_r = 6,81554$, a point that divides into two sections the transitional region, one in which the quantum-classical mixture characterizes a phase-space with more non-chaotic than chaotic curves and other, in which this aspect is reversed [42]. That latter feature is also typical of the classical section. Comparison between figures 4f) (transitional sub-zone) and 4g)–4h) (classical area) exhibits the coherence of the above line of discourse.

Thus, \mathcal{H}_{S_q} as a function of q is perfectly able, by itself, i) of “detecting” important dynamical features like the “Signal Point” $E_r^{\mathcal{P}}$ and ii) of distinguishing between the two transitional sub-regions and registering the similarities between the second of these two and the classical one. Remarkably enough, if we disregard now the transitional zone and just compare the quantal with the classical ones, some similarities and differences are also evidenced. The

facts described in this paragraph demand for the finding of a quantity that might provide one with a way of giving quantitative clothing to the qualitative features just considered.

We propose here that, in this respect, a useful quantity is the \mathcal{H}_{S_q} -curvature (HC)

$$\kappa(q, E_r) = \frac{\left| \frac{\partial^2 \mathcal{H}_{S_q}}{\partial q^2} \right|}{\left(1 + \left(\frac{\partial \mathcal{H}_{S_q}}{\partial q} \right)^2 \right)^{\frac{3}{2}}}. \quad (12)$$

Fig. 5, depicts $\kappa(q_M, E_r)$ vs. E_r , evaluated for that q -value, q_M , minimizing \mathcal{H}_{S_q} (yielding a value $(\mathcal{H}_{S_q})_M$). We appreciate that HC's values differ in our three zones: quantal, transitional, and classical. The three of them are more sharply delineated using the HC κ than by recourse to \mathcal{H}_{S_q} , particularly with regards to the quantum region.

In figures 6 we display the quantities q_M and $(\mathcal{H}_{S_q})_M$ versus E_r . The $(\mathcal{H}_{S_q})_M$ -graph (in which q is different at every E_r) of Fig. 6a) astonishingly resembles those of \mathcal{H}_{S_q} vs. E_r . In turn, q_M (Fig. 6b) behaves clearly as a “demarcator” that performs an exceptionally good job at exhibiting the convergence towards classicality.

One is thus led to the conclusion that it is the parameter q itself the one detecting the quantum-classical transition, via different q -dependent quantities.

4 Conclusions

The focus of attention in this communication has been the classical-quantal frontier, as looked through the glass of a wavelet-band analysis and by recourse to the dynamics governed by a semi-classical hamiltonian that represents the zero-th mode contribution of an strong external field to the production of charged meson pairs. This study is in turn encompassed within Tsallis' statistics.

The highlights of the road towards classicality are described by recourse to the relative energy E_r given by (7). As E_r grows from $E_r = 1$ (the “pure quantum instance”) to $E_r \rightarrow \infty$ (the classical situation), a significant series of *morphology-changes* is detected for the solutions of the system of nonlinear coupled equations (5). The concomitant process takes place in three stages: quantal, transitional, and classic, delimited, respectively, by special values of E_r , namely, E_r^P and E_r^{cl} .

We were able to ascertain that the normalized Tsallis wavelet entropy \mathcal{H}_{S_q} , in the range $0 < q < 5$, correctly describes the dynamical E_r -evolution, unmistakably identifying the above mentioned three stages. As a *second* result we have ascertained that within the subrange $0.1 < q \leq 0.4$, \mathcal{H}_{S_q} , not only *identifies* the three different E_r -regions but also properly portrays the quantum sector, something that Shannon's measure is unable to do. We have thus encountered that the wavelet-constructed \mathcal{H}_{S_q} , in the range $0.1 < q \leq 0.4$, is the most appropriate entropy, and not the orthodox, $q = 1$ of Shannon's.

Thirdly, we find that \mathcal{H}_{S_q} , as a function of q is a good "detector" of transitional features (see Figs. 4): a) identifies $E_r^{\mathcal{P}}$, starting point of the transitional sector and where chaotic behavior begins to emerge and b) distinguishes between the two subsections into which the transitional region divides itself: one in which the quantum-classical mixture characterizes a phase-space with more non-chaotic than chaotic curves and other, in which this aspect is reversed.

Finally, we have discovered other transition-detectors in addition to the normalized Tsallis-entropy, specially its curvature when we plot it for that particular q -value q_M for which \mathcal{H}_{S_q} has a minimum (Fig. 5). q_M itself (Fig. 6b) turns out to a good transition-indicator. These last results affirm that the Tsallis parameter q by itself can be regarded as the "looking glass" through which one can observe the quantum-classical transition.

5 Acknowledgments

AMK are supported by CIC of Argentina.

A Normalized Tsallis wavelet entropy

Wavelet analysis is a suitable tool for detecting and characterizing specific phenomena in time and frequency planes. The *wavelet* is a smooth and quickly vanishing oscillating function with good localization in both frequency and time.

A *wavelet family* $\psi_{a,b}(t) = |a|^{-1/2}\psi\left(\frac{t-b}{a}\right)$ is the set of elementary functions generated by dilations and translations of a unique admissible *mother wavelet* $\psi(t)$. $a, b \in \mathcal{R}$, $a \neq 0$ are the scale and translation parameters respectively, and t is the time. One have a unique analytic pattern and its replications at different scales and with variable time localization.

For special election of the mother wavelet function $\psi(t)$ and for the discrete

set of parameters, $a_j = 2^{-j}$ and $b_{j,k} = 2^{-j}k$, with $j, k \in \mathcal{Z}$ (the set of integers) the family

$$\psi_{j,k}(t) = 2^{j/2} \psi(2^j t - k) \quad j, k \in \mathcal{Z}, \quad (\text{A.1})$$

constitutes an orthonormal basis of the Hilbert space $L^2(\mathcal{R})$ consisting of finite-energy signals.

The correlated *decimated discrete wavelet transform* provides a non-redundant representation of the signal X , and the values $\langle \mathcal{X}, \psi_{a,b} \rangle$ constitute the coefficients in a wavelet series. These wavelet coefficients provide relevant information in a simple way and a direct estimation of local energies at the different scales. Moreover, the information can be organized in a hierarchical scheme of nested subspaces called multiresolution analysis in $L^2(\mathcal{R})$. In the present work, we employ orthogonal cubic spline functions as mother wavelets. Among several alternatives, cubic spline functions are symmetric and combine in a suitable proportion smoothness with numerical advantages.

In what follows, the signal is assumed to be given by the sampled values $\mathcal{X} = \{x(n), n = 1, \dots, N\}$. If the decomposition is carried out over all resolutions levels the wavelet expansion will read ($N_J = \log_2(N)$)

$$\mathcal{S}(t) = \sum_{j=-N_J}^{-1} \sum_k C_j(k) \psi_{j,k}(t) = \sum_{j=-N_J}^{-1} r_j(t), \quad (\text{A.2})$$

where the wavelet coefficients $C_j(k)$ can be interpreted as the local residual errors between successive signal approximations at scales j and $j+1$, and $r_j(t)$ is the *residual signal* at scale j . It contains the information of the signal $\mathcal{S}(t)$ corresponding to the frequencies $2^{j-1}\omega_s \leq |\omega| \leq 2^j\omega_s$.

Since the family $\{\psi_{j,k}(t)\}$ is an *orthonormal* basis for $L^2(\mathcal{R})$, the concept of energy is linked with the usual notions derived from Fourier's theory. The wavelet coefficients are given by $C_j(k) = \langle \mathcal{S}, \psi_{j,k} \rangle$ and the energy, at each resolution level $j = -1, \dots, -N_J$, will be the energy of the detail signal

$$E_j = \|r_j\|^2 = \sum_k |C_j(k)|^2. \quad (\text{A.3})$$

The total energy can be obtained in the fashion

$$E_{tot} = \|\mathcal{S}\|^2 = \sum_{j<0} \sum_k |C_j(k)|^2 = \sum_{j<0} E_j. \quad (\text{A.4})$$

Finally, we define the normalized p_j -values, which represent the *relative wavelet*

energy

$$p_j = E_j / E_{tot} \quad (\text{A.5})$$

for the resolution levels $j = -1, -2, \dots, -N_J$. The p_j yield, at different scales, the probability distribution for the energy. Clearly, $\sum_j p_j = 1$ and the distribution $\{p_j\}$ can be considered as a time-scale density that constitutes a suitable tool for detecting and characterizing specific phenomena in both the time and the frequency planes.

The normalized Tsallis wavelet entropy (NTWE) is just the normalized Tsallis entropy associated to the probability distribution P ,

$$\mathcal{H}_{S_q}[P] = S_q[P]/S_{q,max} = \frac{1}{1 - N_J^{1-q}} \sum_{j=-1}^{-N_J} (p_j - p_j^q), \quad (\text{A.6})$$

where $S_{q,max} = (1 - N_J^{1-q})/(q - 1)$ is attained for the equiprobable distribution $P_e = \{1/N_J, \dots, 1/N_J\}$.

The NTWE appears as a measure of the degree of order/disorder of the time series. It provides useful information about the underlying dynamical process associated with the series. Indeed, a very ordered process can be represented by a periodic mono-frequency signal (signal with a narrow band spectrum). A wavelet representation of such a signal will be resolved at one unique wavelet resolution level, i.e., all relative wavelet energies will be (almost) zero except at the wavelet resolution level which includes the representative series frequency. For this special level the relative wavelet energy will (in our chosen energy units) almost equal unity. As a consequence, the NTWE will acquire a very small, vanishing value. A signal generated by a totally random process or chaotic one can be taken as representative of a very disordered behavior. This kind of signal will have a wavelet representation with significant contributions coming from all frequency bands. Moreover, one could expect that all contributions will be of the same order. Consequently, the relative wavelet energy will be almost equal at all resolutions levels, and the NTWE will acquire its maximum possible value.

References

- [1] C.E. Shannon, *Bell Syst Technol J* 27 (1948) 379; 623.
- [2] J.S. Shiner, M. Davison, P.T. Landsberg, *Phys Rev E* 59 (1999) 1459.
- [3] R. López-Ruiz, H.L. Mancini, X. Calbet, *Phys Lett A* 209 (1995) 321.
- [4] P.W. Lamberti, M.T. Martín, A. Plastino, O.A. Rosso, *Physica A* 334 (2004) 119.
- [5] A.N. Kolmogorov, *Dokl Akad Nauk SSSR* 119 (1958) 861.
- [6] Y.G. Sinai, *Dokl. Akad. Nauk SSSR* 124 (1959) 768.
- [7] M.T. Martín, Ph.D. Thesis. Department of Mathematics, Faculty of Sciences, University of La Plata, La Plata, Argentina, 2004.
- [8] K. Mischaikow, M. Mrozek, J. Reiss, A. Szymczak. *Phys. Rev. Lett.* 82 (1999) 1114.
- [9] G.E. Powell, I.C. Percival, *J. Phys A: Math. Gen.* 12 (1979) 2053.
- [10] O.A. Rosso, M.L. Mairal, *Physica A* 312 (2002) 469.
- [11] R. Hanel, S. Thurner, *Physica A* 380 (2007); G. Kaniadakis, *Phys. Rev. E* 66 (2002) 056125; M. P. Almeida, *Physica A* 300 (2001) 424; J. Naudts, *Physica A* 316 (2002) 323.
- [12] C. Tsallis, *J. Stat. Phys.* 52 (1988) 479.
- [13] P.A. Alemany, D.H. Zanette, *Phys. Rev. E* 49 (1994) R956.
- [14] C. Tsallis, *Fractals* 3 (1995) 541.
- [15] A. Capurro, L. Diambra, D. Lorenzo, O. Macadar, M.T. Martín, C. Mostaccio, A. Plastino, E. Rofman, M.E. Torres, J. Velluti, *Physica A* 257 (1998) 149.
- [16] C. Tsallis, *Phys. Rev. E* 58 (1998) 1442.
- [17] S. Tong, A. Bezerianos, J. Paul, Y. Zhu, N. Thakor, *Physica A* 305 (2002) 619.
- [18] C. Tsallis, C. Anteneodo, L. Borland, R. Osorio, *Physica A* 324 (2003) 89.
- [19] O.A. Rosso, M.T. Martín, A. Plastino, *Physica A* 320 (2003) 497.
- [20] L. Borland, *Europhys. News* 36 (2005) 228.
- [21] H. Huang, H. Xie, Z. Wang, *Phys. Lett. A* 336 (2005) 180.
- [22] D.G. Pérez, L. Zunino, M.T. Martín, M. Garavaglia, A. Plastino, O. A. Rosso, *Phys. Lett. A* 364 (2007) 259.
- [23] M. Kalimeri, C. Papadimitriou, G. Balasis, K. Eftaxias, *Physica A* 387 (2008) 1161.

- [24] J.P. Paz and W.H. Zurek, Phys. Rev. Lett. 82 (1999) 5181.
- [25] J. Emerson and L.E. Ballentine, Phys. Rev. E 64 (2001) 016217.
- [26] A.M. Kowalski, M.T. Martin, A. Plastino, and A.N. Proto, Int. J. of Bifurcation and Chaos 13 (2003) 2315.
- [27] A.M. Kowalski, M.T. Martin, A. Plastino, A.N. Proto and O.A. Rosso, Phys. Lett. A 311 (2003) 180.
- [28] A.M. Kowalski, M.T. Martin, A. Plastino and O.A. Rosso, Int. J. Mod. Phys. B 19 (2005) 2273.
- [29] F. Bloch, Phys. Rev. 70 (1946) 460.
- [30] P. Meystre, M. Sargent III, Elements of Quantum Optics, Springer-Verlag, New York/Berlin, 1991.
- [31] G.F. Bertsch, Phys. Rev. Lett. 95B (1980) 157.
- [32] A. Bulgac, Phys. Rev. C 40 (1989) 1073.
- [33] P.W. Milonni, J. R. Ackerhalt, H.W. Galbraith, Rev. Lett. 50 (1980) 966.
- [34] P.W. Milonni, M.L. Shih, J. R. Ackerhalt, Chaos in Laser-Matter Interactions, World Scientific Publishing Co., Singapore, 1987.
- [35] G. Kociuba N. R. Heckenberg, Phys. Rev. E 66 (2002) 026205.
- [36] P. Ring, P. Schuck, The Nuclear Many-Body Problem, Springer-Verlag, New York/Berlin, 1980.
- [37] L. L. Bonilla, F. Guinea, Phys. Lett. B 271 (1991) 196; Phys. Rev. A 45 (1992) 7718.
- [38] F. Cooper, S. Habib, Y. Kluger, E. Mottola, Phys. Rev. D 55 (1997) 6471.
- [39] F. Cooper, J. Dawson, S. Habib, R. D. Ryne, Phys. Rev. E 57 (1998) 1489.
- [40] D. J. H. Chung, Phys. Rev. D 67 (2003) 083514.
- [41] A. M. Kowalski, M. T. Martin, J. Nuñez, A. Plastino, A. N. Proto, Physica A 276 (2000) 95; Phys. Rev. A 58 (1998) 2596.
- [42] A.M. Kowalski, A. Plastino, A.N. Proto, Phys. Lett. A 297 (2002) 162.
- [43] A.M. Kowalski, M.T. Martin, A. Plastino and O. A. Rosso, Physica D 233 (2007) 21.
- [44] L. Zunino, D.G. Pérez, A. Kowalski, M.T. Martín, M. Garavaglia, A. Plastino, O.A. Rosso, Physica A 387 (2008) 6057.

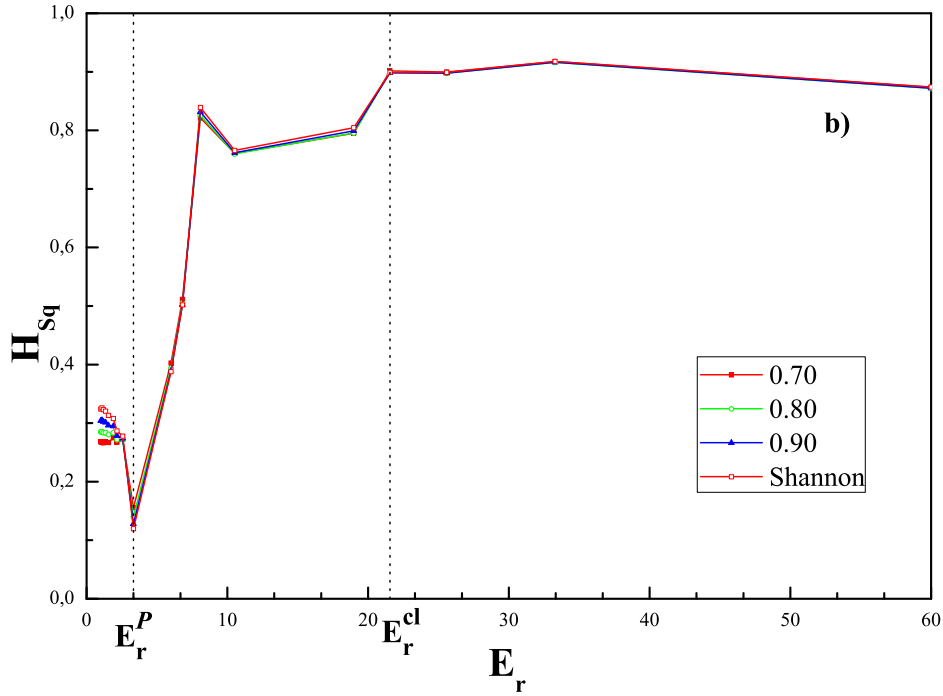
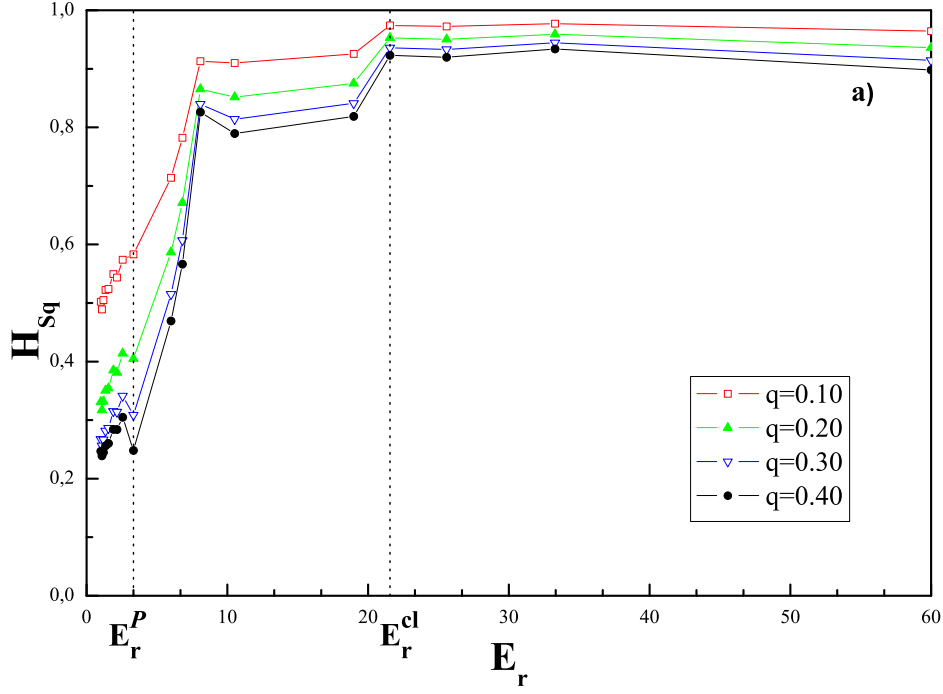


Fig. A.1. Normalized Tsallis entropy \mathcal{H}_{S_q} vs. E_r for $q < 0.7$ (Fig. 1a) and $0.7 \leq q < 1$ (Fig. 1b). Shannon's entropies are also displayed. Three zones are to be differentiated. They are delimited by special E_r -values, namely, $E_r^P = 3.3282$ and $E_r^{cl} = 21,55264$. Note that the quantum sector is that for which $1 \leq E_r < E_r^P$ and, there, \mathcal{H}_{S_q} 's slope changes with q , being negative for $q > 0.7$ (Figs. 1b) and positive for $0 < q < 0.7$, if $E_r \leq 2.6$ (Figs. 1a). For $0.1 < q \leq 0.4$, \mathcal{H}_{S_q} -values are in the quantal zone smaller than (or equal to) in the transitional one.

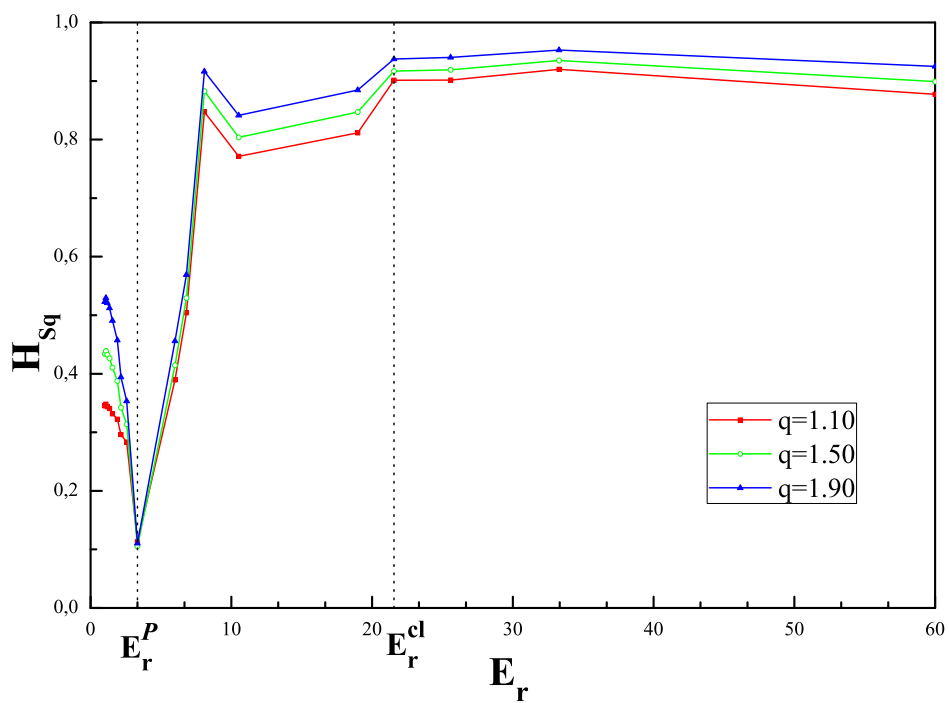


Fig. A.2. Normalized Tsallis entropy \mathcal{H}_{S_q} vs E_r for $1 < q \leq 2$. The three zones of Fig. 1 are also seen here.

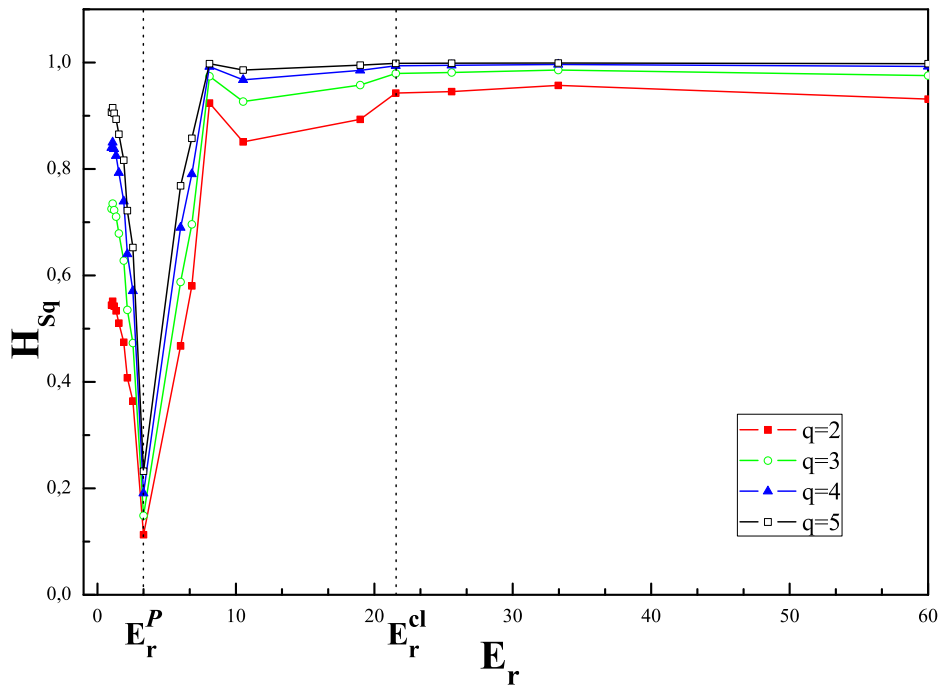


Fig. A.3. Normalized Tsallis entropy \mathcal{H}_{S_q} vs. E_r for $2 \leq q \leq 5$. In the range $1 < q < 3$ the morphology is that of Fig. 1. For $3 \leq q < 5$, the \mathcal{H}_{S_q} -curve starts acquiring a “horizontal” nature in the transition region close to the classical one. For $q > 5$, a “merging” between the two sectors takes place.

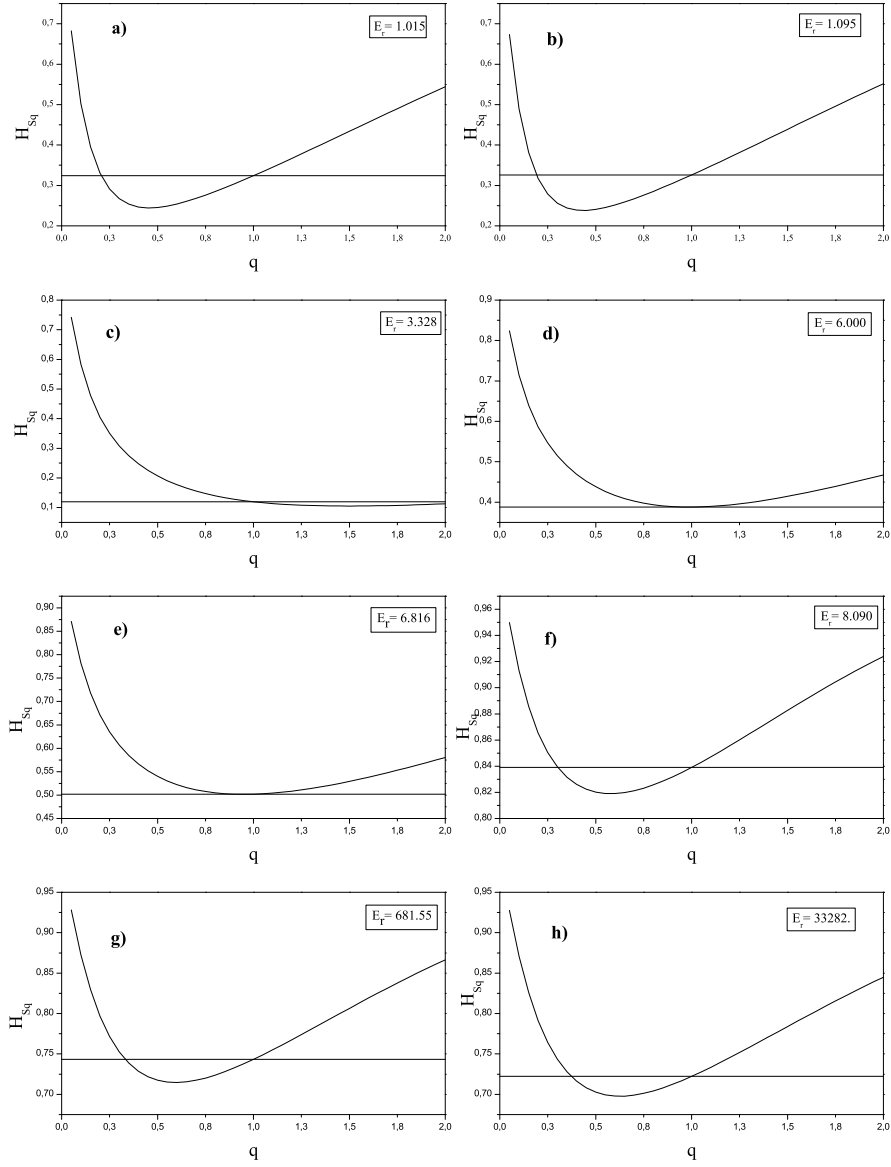


Fig. A.4. Normalized Tsallis entropy \mathcal{H}_{S_q} vs. q for different E_r -values. 1) Quantal (Figs. 4a - 4b), transitional (Figs. 4c, 4d, 4e and 4f) and classic (4g - 4h). The corresponding Shannon entropy value (horizontal line) is included in all graphs for comparison's purpose. Note that \mathcal{H}_{S_q} intersects the Shannon entropy-curve for $q > 1$ in figure 4c) and becomes tangent to it in figures 4d) - 4e).

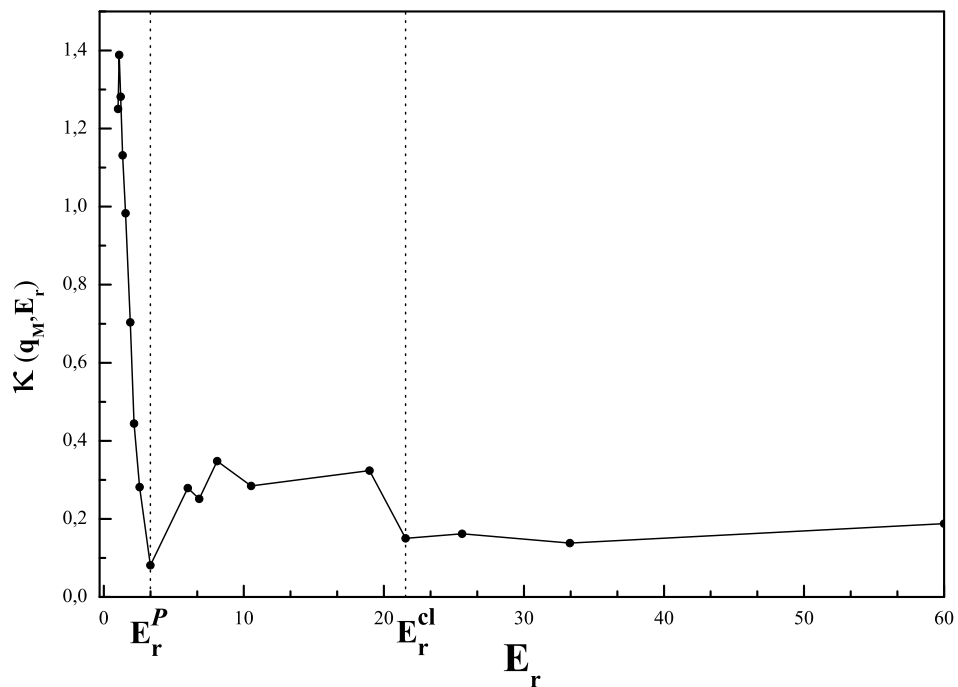


Fig. A.5. We depict the curvature $\kappa(q_M, E_r)$ vs. E_r . At $q = q_M$ \mathcal{H}_{S_q} adopts its minimum value. The three regions of Fig. 1 are clearly delineated.

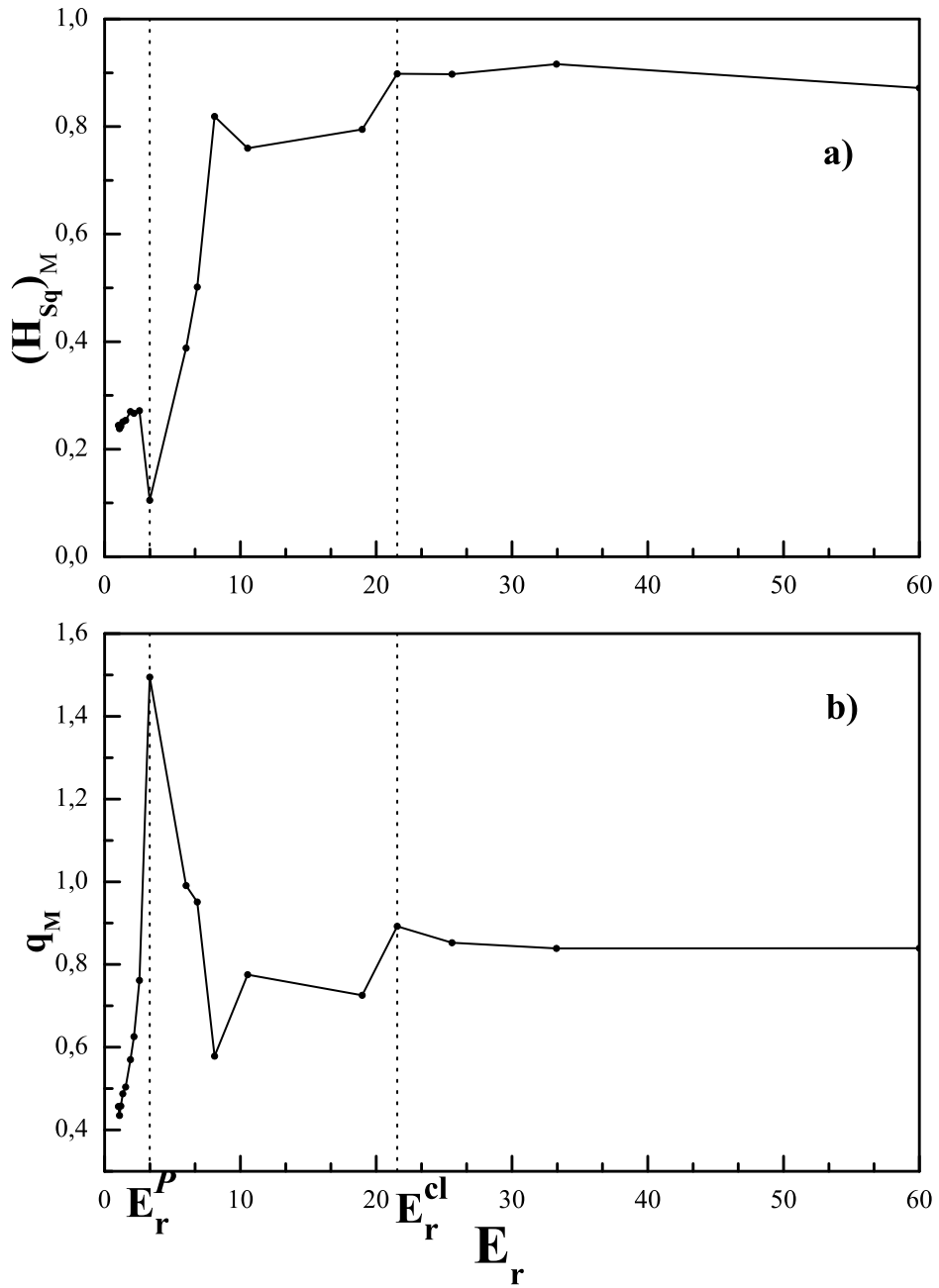


Fig. A.6. 6a) Graph of $(\mathcal{H}_{S_q})_M$, the minimum \mathcal{H}_{S_q} -value, versus E_r . 6b) q_M , the particular q -value at which that minimum is attained versus E_r . The two plots display the quantum-classical transition.